Rare-Earth Free Motor with Field Poles Excited by Space Harmonics

― Current Phase-Torque Characteristics of Self-Excitation Synchronous Motor ―

Masahiro Aoyama

Department of Environment and Energy System,
Graduate School of Science and Technology,
Shizuoka University
3-5-1 Johoku, Naka-Ku, Hamamatsu,
Shizuoka 432-8561, Japan
Electric Drive Vehicle Design Department
Suzuki Motor Corporation
aoyamam@hhq.suzuki.co.jp

Toshihiko Noguchi

Department of Electrical and Electronic Engineering,
Graduate School of Engineering,
Shizuoka University
3-5-1 Johoku, Naka-Ku, Hamamatsu,
Shizuoka 432-8561, Japan
ttnogut@ipc.shizuoka.ac.jp

Abstract— This paper describes a synchronous motor in which space harmonics power is utilized for field magnetization instead of permanent magnets. The stator has a concentrated winding structure, and the rotor has two sorts of windings, i.e., an induction pole (I-pole) winding that retrieves mainly the third space harmonics power and an excitation pole (E-pole) winding for the field magnetization. The both coils are connected via a diode rectifying circuit. The optimum placement of the I-pole on the rotor is mathematically discussed and is analytically determined through FEM based computer simulations. In addition, it is clarified that the E-pole torque becomes larger as the fundamental synchronous speed rises and that the MTPA control angle advances with increase of the speed.

Keywords—component; synchronous motor, self-excitation, wound-field, induced current, field current, electromagnets

I.   INTRODUCTION

In recent years, hybrid vehicles (HEVs) and electric vehicles (EVs) driven by shared power with an internal-combustion engine or only by electric power are focused on because of environmental concerns such as global warming, exhaustion of fossil fuels, and air pollution problems. An electric machine is one of the key components in the HEVs and the EVs from the viewpoint of dynamic drivability and fuel consumption performance. Traction motors for the HEVs have remarkably unique features, compared with industry applied motors. Wide adjustable speed drive range, high maximum torque, and high power density without sacrificing its efficiency are demanded to improve the total automotive system efficiency. In general, an IPM (Interior Permanent Magnet) motor is applied to the HEVs owing to its highly improved efficiency and specific power capability per physical size. Permanent magnets used for the IPM motor are very expensive because Nd-Fe-B magnets are commonly employed to realize high power density and to improve fuel efficiency at low-load operation for a street use. Moreover, the traction motors are usually installed on the chassis where special

countermeasures must be taken for environmental and thermal issues. In order to mitigate demagnetization caused by temperature rise of the permanent magnets for example, extremely expensive rare-earth metals such as Dy and Tb must be added to the Nd-Fe-B magnets.

Various rare-earth-less and rare-earth-free motors are recently proposed due to remarkable rise of the Nd-Fe-B magnet market prices and a global maldistribution problem of the magnet additives like Dy and Tb. Wound-field motors that replace such permanent magnets with electromagnets are intensively investigated both in industries and in academia as post IPM motors [1][2]. For example, a separate excitation wound-field synchronous motor is proposed in [1]. This motor is capable to utilize armature reaction torque by wound-field torque, and the field magnetization control allows high efficiency operation. An external chopper circuit is, however, indispensable for the wound-field winding. Furthermore, it is rather difficult to transfer the field magnetization power from the primary to the secondary, and an extra copper loss in the wound-field winding is also a serious concern. Therefore, a self-excitation technique proposed in [3][4] is reevaluated by the authors to solve the problems regarding the separate excitation wound-field motors. The classic self-excitation based synchronous motor has a stator with distributed windings and a salient pole rotor with a single winding connected via a half-bridge rectifier. The second space harmonics linking to the rotor winding is utilized for the field magnetization. However, low space harmonics power transfer to the rotor winding makes it difficult to improve the motor efficiency further. In addition, it is rather difficult to retrieve efficiently the space harmonics power because the single rotor winding plays both roles of an induction coil and an electromagnet coil at the same time.

In this paper, the drawbacks of the classic self-excited synchronous motor are solved, and a new configuration and a new operation mechanism of the self-excitation are proposed,
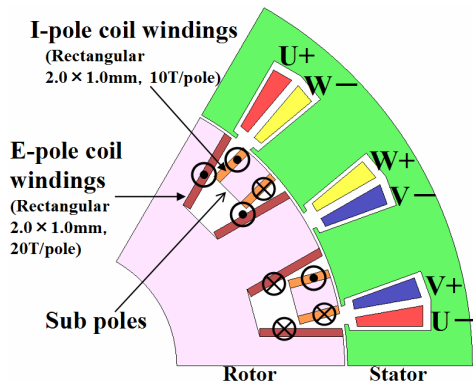
I-pole coil windings
(Rectangular 2.0 × 1.0mm, 10T/pole)

E-pole coil windings
(Rectangular 2.0 × 1.0mm, 20T/pole)

Sub poles

Rotor   Stator

Fig. 1.   Cross section diagram of proposed motor.

TABLE I   SPECIFICATION OF MOTOR.

Number of poles	12
Number of slots	18
Stator outer diameter	200 mm
Rotor diameter	138.6 mm
Axial length of core	54 mm
Air gap length	0.7 mm
Maximum current	273 A$_{pk}$
Stator winding resistance	32.1 mΩ / phase
Number of coil-turn	48
Winding connection	6 parallel
I-pole winding resistance	12.1 mΩ / pole
E-pole winding resistance	26.9 mΩ / pole
Thickness of iron core steel plate	0.35 mm

focusing on the space harmonics power in the motor. Furthermore, it is mathematically explained that the third space harmonics power can mainly be retrieved for the field magnetization power. In addition, current phase-torque characteristics as well as adjustable speed drive characteristics are presented by the FEM based magnetic field analysis.

II.   MATHEMATICAL ANALYSIS OF SELF-EXCITATION

A. Configuration of New Self-Excitaion Wound-Field Motor

Figure 1 shows a cross section diagram of the proposed motor (self-excitation wound-field motor) where the wound-field coils are added to the rotor salient poles, and the induction coils are placed in spaces between the rotor salient poles, i.e., rotor slots. Conventional common motors such as a synchronous reluctance motor (SynRM) dissipate the space harmonics power caused by the stator with the concentrated winding structure, whereas the proposed motor positively takes advantage of the space harmonics power for the field magnetization. Each of an induction pole (I-pole) is a special pole exclusively used for the magnetizing power generation from the third space harmonics. On the other hand, each excitation pole (E-pole) is a salient pole on the rotor for the field excitation, which uses the retrieved third space harmonics
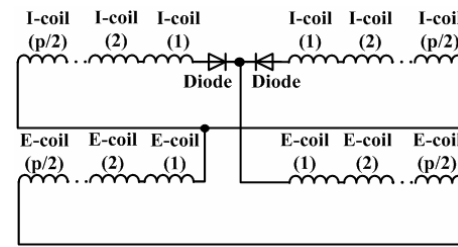

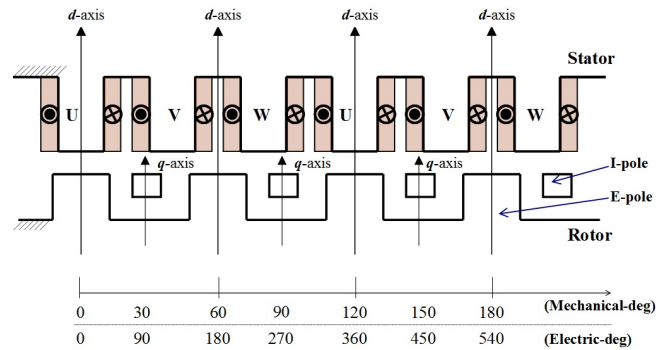Fig. 2.   Rotor winding connection diagram using full-bridge rectifier.

Fig. 3.   Developed salient pole model of proposed motor.

power. Every I-pole and E-pole is connected in series via a diode rectifying circuit as shown in Fig. 2, where p indicates a pole number. Specifications of the motor shown in Fig. 1 are listed in Table I.

B. Mathematical Model on dq-Reference Frame

A mathematical model of the proposed motor is established in this section followed by the analysis result of I-pole optimum placement design on the rotor. The operation principle of the proposed motor can be explicated by voltage equations on the synchronous rotating reference frame. Figure 3 shows a developed salient pole model of the motor. As can be seen in the figure, the rotor salient pole is aligned with the d-axis, and the q-axis is supposed to be between the two salient poles. Assuming a combination between the rotor pole counts and the stator slot counts is 2 to 3, a U-phase self inductance L_u can be given by

$$L_U(\theta) = L_{S0} + L_S \cos 2\theta , \qquad (1)$$

where L_{S0} is a constant part and L_S is an amplitude of the periodical variation of the self inductance. Similarly, V-phase self inductance L_V and W-phase self inductance L_W can be given by

$$L_V(\theta) = L_{S0} + L_S \cos\left(2\theta - \frac{2}{3}\pi\right) \text{ and} \qquad (2)$$

$$L_W(\theta) = L_{S0} + L_S \cos\left(2\theta + \frac{2}{3}\pi\right), \text{ respectively.} \qquad (3)$$

An α-axis self inductance $L_α$ and a β-axis self inductance $L_β$ on the stationary orthogonal reference frame are obtained by a coordinate transform from three-phase to two-phase as follows:

$$L_\alpha(\theta) = L_U(\theta) + L_V(\theta)\cos\frac{2}{3}\pi + L_W \cos\frac{4}{3}\pi = \frac{3}{2}L_S \cos 2\theta \text{ and} \qquad (4)$$

$$L_\beta(\theta) = L_V(\theta)\sin\frac{2}{3}\pi + L_W\sin\frac{4}{3}\pi = -\frac{3}{2}L_S\sin 2\theta \ . \tag{5}$$

Applying a rotational coordinate transform to the above equations by using a d-axis phase θ_d and a q-axis phase θ_q expressed by Eq. (6), a d-axis self inductance L_d and a q-axis self inductance L_q can be obtained as Eqs. (7) and (8):

$$\theta_d = \omega t, \ \theta_q = \omega t - \frac{\pi}{2} , \tag{6}$$

$$L_d = \frac{3}{2}L_S\cos 2\omega t , \text{ and} \tag{7}$$

$$L_q = \frac{3}{2}L_S\sin 2\omega t , \tag{8}$$

where ω is an electrical synchronous angular frequency.

The mathematical model of the proposed motor can be expressed as the following voltage equation:

$$\begin{bmatrix} v_{sd} \\ v_{sq} \end{bmatrix} = \begin{bmatrix} R_s & 0 \\ 0 & R_s \end{bmatrix}\begin{bmatrix} i_{sd} \\ i_{sq} \end{bmatrix} + \begin{bmatrix} p & -\omega \\ \omega & p \end{bmatrix}\begin{bmatrix} \psi_{sd} \\ \psi_{sq} \end{bmatrix}$$
$$= \begin{bmatrix} R_s & 0 \\ 0 & R_s \end{bmatrix}\begin{bmatrix} i_{sd} \\ i_{sq} \end{bmatrix} + \begin{bmatrix} p & -\omega \\ \omega & p \end{bmatrix}\begin{bmatrix} L_d & 0 & M_d & 0 \\ 0 & L_q & 0 & M_q \end{bmatrix}\begin{bmatrix} i_{sd} \\ i_{sq} \\ i_{rd} \\ i_{rq} \end{bmatrix}, \tag{9}$$

where v_{sd}, v_{sq}, i_{sd} and i_{sq} are armature voltages and currents, i_{rd} and i_{rq} are a d-axis and a q-axis rotor winding currents, R_s is an armature winding resistance, M_d and M_q are a d-axis and a q-axis mutual inductances, and p denotes a differential operator, respectively. The I-pole is an auxiliary pole to generate an induced current by retrieving the space harmonics power of the motor, and is designed to be magnetically independent of the main magnetic flux path; thus, i_{rq}=0. On the other hand, the self inductances on the dq-reference frame are constants because both of the stator and the rotor rotate at the synchronous angular frequency ω with the dq-reference frame. However, the mutual inductance varies periodically with respect to the time because a mechanical phase displacement between the armature windings and the I-pole windings changes according to the rotation; hence, Eq. (9) is rewritten as the following expression:

$$\begin{bmatrix} v_{sd} \\ v_{sq} \end{bmatrix} = \begin{bmatrix} R_s & 0 \\ 0 & R_s \end{bmatrix}\begin{bmatrix} i_{sd} \\ i_{sq} \end{bmatrix} + \begin{bmatrix} L_d & 0 & M_d \\ 0 & L_q & 0 \end{bmatrix}p\begin{bmatrix} i_{sd} \\ i_{sq} \\ i_{rd} \end{bmatrix}$$
$$+ \begin{bmatrix} 0 & 0 & pM_d \\ 0 & 0 & 0 \end{bmatrix}\begin{bmatrix} i_{sd} \\ i_{sq} \\ i_{rd} \end{bmatrix} + \omega\begin{bmatrix} 0 & -L_q & 0 \\ L_d & 0 & M_d \end{bmatrix}\begin{bmatrix} i_{sd} \\ i_{sq} \\ i_{rd} \end{bmatrix} . \tag{10}$$

Ignoring a leakage inductance, the mutual inductance M_d can simply be expressed as

$$M_d = \frac{N_{rd}}{N_S}L_d = \frac{3}{2}\frac{N_{rd}}{N_S}L_S\cos 2\omega t , \tag{11}$$

where N_{rd} and N_S are the numbers of turns of the d-axis rotor winding and the stator windings, respectively. Therefore, the

time derivative of M_d in the third term of Eq. (10) is calculated as follows:

$$pM_d = p\left(\frac{N_{rd}}{N_S}L_d\right) = -3\omega\frac{N_{rd}}{N_S}\sin 2\omega t = -2\omega\frac{N_{rd}}{N_S}L_q . \tag{12}$$

Consequently, the mathematical model of the proposed motor can be obtained as

$$\begin{bmatrix} v_{sd} \\ v_{sq} \end{bmatrix} = \begin{bmatrix} R_s & 0 \\ 0 & R_s \end{bmatrix}\begin{bmatrix} i_{sd} \\ i_{sq} \end{bmatrix} + \begin{bmatrix} L_d & 0 & \frac{N_{rd}}{N_S}L_d \\ 0 & L_q & 0 \end{bmatrix}p\begin{bmatrix} i_{sd} \\ i_{sq} \\ i_{rd} \end{bmatrix}$$
$$+ \omega\begin{bmatrix} 0 & -L_q & -2\frac{N_{rd}}{N_S}L_q \\ L_d & 0 & \frac{N_{rd}}{N_S}L_d \end{bmatrix}\begin{bmatrix} i_{sd} \\ i_{sq} \\ i_{rd} \end{bmatrix} . \tag{13}$$

The first term of the above equation is a voltage drop by the armature winding resistance, the second term is a transformer electromotive force, and the third term corresponds to an electromotive force.

C. Mathematical Discussion on I-pole Optimum Placement

Assuming that the U-phase armature current is given as

$$i_U(t) = I_S\cos(\omega t + \beta), \tag{14}$$

where β is a current phase, a magnetic flux of the U-phase $\varphi_{S\text{-}U}$ is derived as

$$\phi_{S-U} = \frac{L_U(\theta)i_U(t)}{N_S} = \frac{\{L_{S0}+L_S\cos 2\theta\}I_S\cos(\omega t + \beta)}{N_S} . \tag{15}$$

Other magnetic fluxes of the V-phase and the W-phase can similarly be derived as

$$\phi_{S-V} = \frac{\left\{L_{S0}+L_S\cos\left(2\theta - \frac{2}{3}\pi\right)\right\}I_S\cos\left(\omega t + \beta - \frac{2}{3}\pi\right)}{N_S} \text{ and} \tag{16}$$

$$\phi_{S-W} = \frac{\left\{L_{S0}+L_S\cos\left(2\theta + \frac{2}{3}\pi\right)\right\}I_S\cos\left(\omega t + \beta + \frac{2}{3}\pi\right)}{N_S} . \tag{17}$$

Therefore, the total three-phase armature flux is calculated as follows:

$$\phi_{S-UVW} = \phi_{S-U} + \phi_{S-V} + \phi_{S-W}$$
$$= \frac{3}{2}\frac{1}{N_S}L_S I_S\cos(\omega t + \beta - 2\theta) . \tag{18}$$

An α-axis magnetic flux $\varphi_{S\text{-}\alpha}$ and a β-axis magnetic flux $\varphi_{S\text{-}\beta}$ on the stationary orthogonal reference frame are obtained by the following rotational coordinate transform:

$$\phi_{S-\alpha} = \phi_{S-U} + \phi_{S-V}\cos\frac{2}{3}\pi + \phi_{S-W}\cos\frac{4}{3}\pi$$
$$= \frac{I_S}{N_S}\left[\frac{1}{2}L_{S0}\{3\cos(\omega t + \beta)+\sqrt{3}\sin(\omega t + \beta)\} - \frac{1}{4}L_S\cos(\omega t + \beta - 2\theta)\right]$$
$$\text{and} \tag{19}$$

$$\phi_{S-\beta} = \phi_{S-V} \sin\frac{2}{3}\pi + \phi_{S-W} \sin\frac{4}{3}\pi$$
$$= \frac{3}{2}\frac{I_S}{N_S}\left[L_{S0}\sin(\omega t+\beta)+\frac{1}{2}L_S\sin(\omega t+\beta+2\theta)\right]. \tag{20}$$

Applying a rotational coordinate transform to the above equations by using the d-axis phase θ_d and the q-axis phase θ_q expressed in Eq. (6), the d-axis magnetic flux φ_{S-d} and the q-axis magnetic flux φ_{S-q} are obtained as Eqs. (21) and (22),

$$\phi_{S-d} = \frac{I_S}{N_S}\left[\frac{1}{2}L_{S0}\left\{3\cos(\omega t+\beta)+\sqrt{3}\sin(\omega t+\beta)\right\}-\frac{1}{4}L_S\cos(-\omega t+\beta)\right]$$

and $\tag{21}$

$$\phi_{S-q} = \frac{3}{2}\frac{I_S}{N_S}\left[L_{S0}\sin(\omega t+\beta)+\frac{1}{2}L_S\sin(3\omega t+\beta)\right]. \tag{22}$$

An induced voltage is caused in the rotor winding by the magnetic flux linkages of the d-axis and the q-axis expressed by Eqs. (21) and (22). For simplification of the calculation, a cross-linkage magnetic flux and a leakage magnetic flux are ignored. Since the dq-reference frame rotates synchronously at the angular frequency ω, the rotor winding and the d-axis and the q-axis magnetic fluxes cause magnetic coupling of the higher frequency than the synchronous speed. Therefore, Eqs. (21) and (22) show that the space harmonics magnetic path is established on the q-axis. In addition, Eq. (22) shows that the field magnetization energy for the self-excitation is mainly obtained from the third space harmonics.

Figure 4(a) shows a magnetic flux vector and flux lines of the third space harmonics simulated by the FEM based magnetic field analysis. As shown in the figure, the third space harmonics magnetic flux mainly flows through a slot part between the rotor salient poles, of which direction corresponds to the q-axis, and leaks to the salient poles on the d-axis. Therefore, the third space harmonics power can efficiently be retrieved by placing sub-poles on the q-axis as shown in Fig. 4(b). Figure 5 shows the induced current under MTPA (Max Torque Per Ampere) control of the series connected I-pole winding in forward direction of the diode rectifying circuit. As can be seen in the figure, the induced current of the proposed motor is much higher than that of the model without the sub-poles, which demonstrates effectiveness of the optimum placement design of the sub-poles.

Ignoring a leakage magnetic flux, the induced voltage of the I-pole generated by the linkage of the third space harmonics is given by

$$v_{rq} = N_{rq}\mathrm{p}\left(\frac{3}{4}\frac{L_S I_S}{N_S}\sin(3\omega t+\beta)\right) = \omega\left(\frac{9}{4}\frac{N_{rq}}{N_S}L_S I_S\right)\cos(3\omega t+\beta). \tag{23}$$

This electromotive force is applied across the E-pole windings via the diode rectifier. I_{rd} is considered with two terms of constant part and the 6th periodical variation part with Fourier series development of full-bridge rectification of Eq. (23).

D. Electromagnet Torque by Self-Excitation

The output torque of the proposed motor is obtained by the
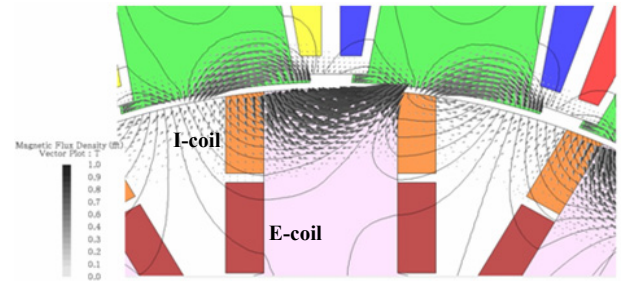
(a) Without sub-poles.
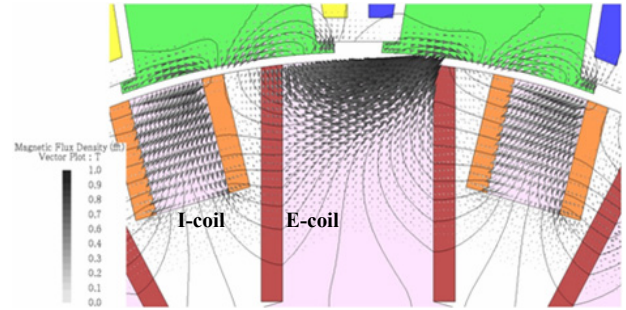
(b) With sub-poles (Proposed model).
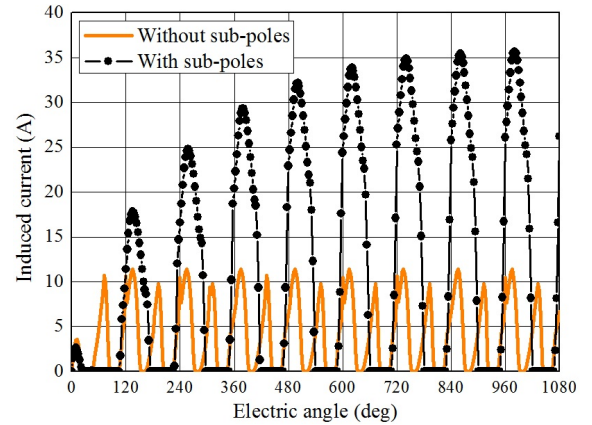Fig. 4. Third space harmonics vector and flux lines.

Fig. 5. Induced current waveforms in forward direction.

vector product between the armature current and the magnetic flux which is described in a part of the third term of Eq. (13). The output torque is expressed as

$$T = P_p\begin{bmatrix}i_{sd} & i_{sq}\end{bmatrix}\begin{bmatrix}0 & -L_q & -2\dfrac{N_{rd}}{N_s}L_q \\ L_d & 0 & \dfrac{N_{rd}}{N_s}L_d\end{bmatrix}\begin{bmatrix}i_{sd} \\ i_{sq} \\ i_{rd}\end{bmatrix},$$

$$= \left(L_d - L_q\right)i_{sd}i_{sq} + \frac{N_{rd}}{N_S}\left(L_d i_{sq} - 2L_q i_{sd}\right)i_{rd} \tag{24}$$

where P_p is a pole-pair number. As expressed in the above equation, the output torque is composed of two terms, i.e., reluctance torque and electromagnet torque. The former is basically independent of the operation angular frequency ω. The field current to generate the electromagnet torque, however, is proportional to ω because the voltage applied to

the E-pole is given by the full-bridge rectification of Eq. (23). In addition, it is found that the electromagnet torque includes the *dq*-axes inductances and the winding turn ratio between the stator and the rotor as indicated in Eq. (24).

III. CURRENT PHASE-TORQUE CHARACTERISTICS

A. Current Phase-Torque Characteristics

Figure 6 shows current phase-torque (average torque in the steady state) characteristics at 1000 r/min of the proposed motor calculated by the FEM based computer simulations. Separation of the reluctance torque and the electromagnet torque is performed through the following steps:

1) Calculation of the reluctance torque at a current phase of 45 deg without connecting the rotor windings,

2) Determination of the current phase-reluctance torque characteristic by fitting a sin2β trigonometric function of which amplitude is the torque value at 45 deg calculated at the previous step,

3) Calculation of the current phase-total torque characteristic with the rotor windings connected, and

4) Subtraction of the reluctance torque from the total torque to obtain the electromagnet torque separately.

As shown in Fig. 6, the electromagnet torque, i.e., an additional torque generated by the self-excitation using the space harmonics, is enlarged as the armature current becomes higher. A ratio between the reluctance torque and the electromagnet torque varies with the armature current. This is because that the third space harmonics retrieved mainly for the field magnetization power increase with the armature current as expressed by Eq. (22). Figure 7 shows the I-pole induced current waveforms in the forward direction of the diode rectifier at a constant speed of 1000 r/min. It is confirmed in the figure that the higher induced current is generated as the armature current becomes higher. Figure 8 shows the field current characteristics at 1000 r/min. The field current is formed by the full-bridge diode rectification of the induced current and its average is almost proportional to the armature current.

B. Adjustable Speed Drive Characteristics

Figure 9 shows adjustable speed drive characteristics of the proposed motor. As indicated by Eq. (24), the higher electromagnet torque is delivered as the synchronous speed increases because the self-excited E-coil torque is proportional to the speed. The MTPA control angle advances with the increase of the speed. Figures 10 and 11 are the induced and the field current waveforms with respect to the rotation speed. Also, these figures show transient responses from an initial standstill condition of the rotor. As can be seen in Fig. 11, the transient behavior takes a longer time as the rotating speed increases because the inductance of the E-pole varies as a function of the rotating speed. On the other hand, the higher E-coil torque which is delivered as the synchronous speed increases is limited by the magnetic saturation of the rotor or stator teeth.
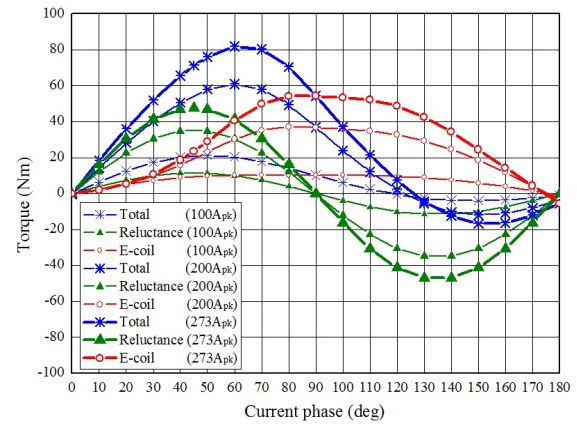

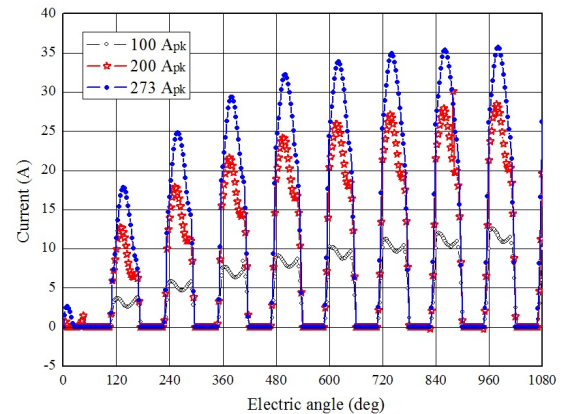Fig. 6. Current phase-torque characteristics at 1000 r/min.
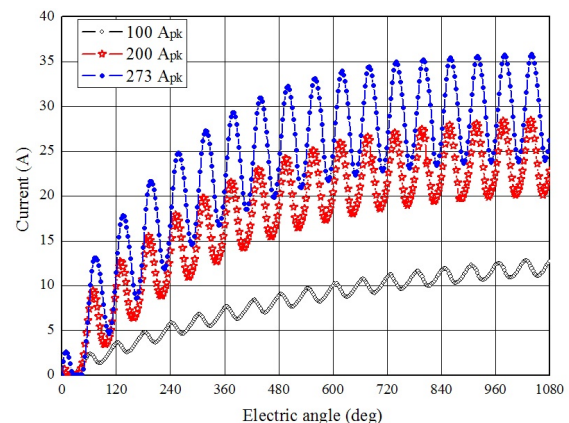

Fig. 7. Induced current characteristics at 1000 r/min.

Fig. 8. Field current characteristics at 1000 r/min.

IV. CONCLUSION

This paper has proposed a new rare-earth-less motor that can utilize space harmonics power for the field magnetization instead of permanent magnets. By splitting the rotor winding into the induction pole (I-pole) winding and the excitation pole (E-pole) winding and by rectifying the induced current with a full-bridge diode rectifier, the space harmonics power can efficiently be retrieved and the total output torque can effectively be enhanced by the extra electromagnet torque. In
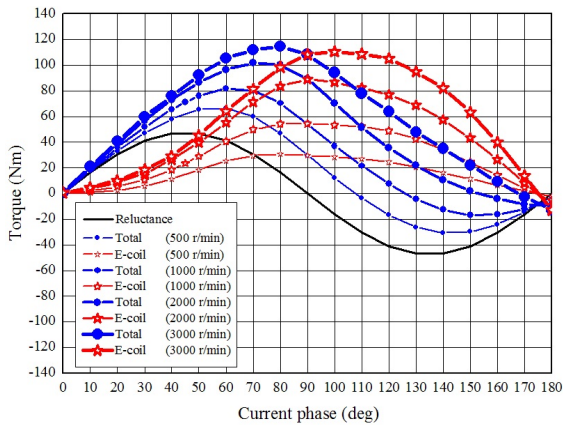
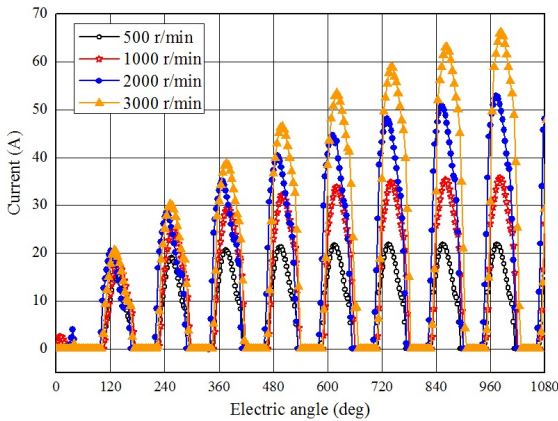Fig. 9. Current phase-torque characteristics at 273 A_{pk}.

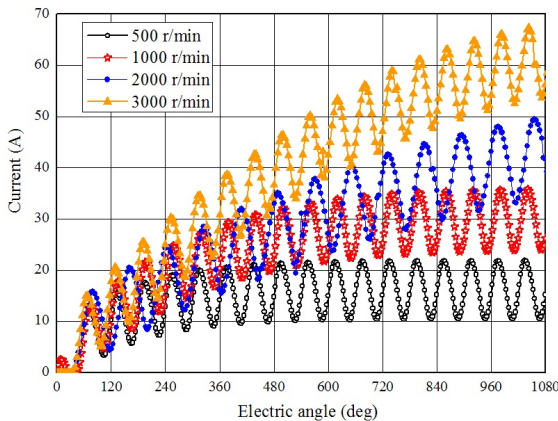Fig. 10. Induced current characteristics at 273 A_{pk}.

Fig. 11. Field current characteristics at 273 A_{pk}.

addition, it has mathematically been proven that the third space harmonics are the main source of the field magnetization power. Furthermore, the current phase-torque characteristics and the adjustable speed drive characteristics have been presented by FEM based electromagnetic analyses. The electromagnet torque generated by the I-poles and the E-poles on the rotor takes significant part of the total output torque. The future work of this study is to setup an actual prototype machine to verify the theoretical discussion and the analysis
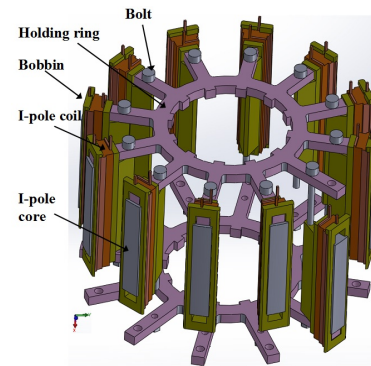

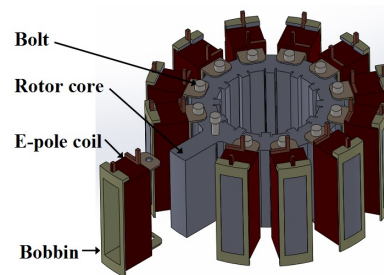Fig. 12. Mechanical configuration of I-pole unit.

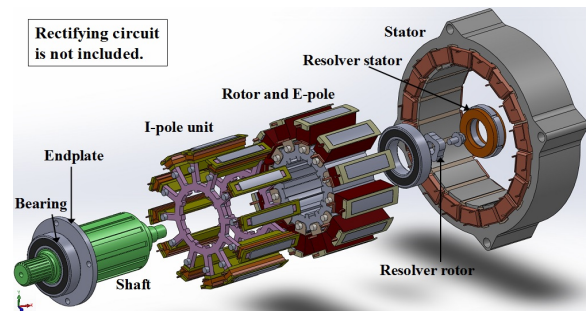Fig. 13. Mechanical configuration of rotor and E-pole.

Fig. 14. Mechanical configuration of proposed motor.

results through experimental tests. Figures 12-14 illustrate three-dimensional component exploded views of the prototype to be produced. The I-poles are firmly implemented with a pair of the holding ring plates so that the I-poles are settled in the rotor slots.

REFERENCES

[1] M. Azuma, M. Hezeyama, M. Morita, Y. Kuroda, and M. Inoue, "Driving Characteristics of a Claw Pole Motor Using Filed Excitation for Hybrid Electric Vehicles," IEEJ Technical Meeting on Vehicle Technology, pp. 37-40, 2011 (in Japanese).

[2] T. Kosaka, T. Hirose, N. Matsui, and K. Elissa, "Some Considerations on Experimental Drive Characteristics of Less Rare-Earth HEM," IEEJ Transactions on Industry Applications, no.1-O6-2, pp. 85-90, 2011 (in Japanese).

[3] S. Nonaka, "The Self-Excited Type Single-Phase Synchronous Motor," IEEJ Transactions on Industry Applications, vol.78, no. 842, pp. 1430-1438, Nov. 1958 (in Japanese).

[4] S. Nonaka, and K. Akatsu, "Analysis of New Brushless Self-Excited Single-Phase Synchronous Generator by Finite Element Method," IEEJ Transactions on Industry Applications, vol.30, no.3, pp.615-620, 1994.